

# Machine Learning for Identifying Characteristics of Isolated, Clustered, and Pulsed Vapor Bubbles on a Heated Surface under Non-Stationary Boiling Conditions

P.V. Khan<sup>1,2\*</sup>, A.A. Levin<sup>1,2</sup>, I.I. Chupin<sup>1,2</sup>, A.S. Safarov<sup>2</sup>

<sup>1</sup>Novosibirsk State University, Novosibirsk, Russia

<sup>2</sup>Melentiev Energy Systems Institute of Siberian Branch of Russian Academy of Sciences, Irkutsk, Russia

**Abstract** — This paper presents an automated system for analyzing high-speed video of non-stationary nucleate boiling on an opaque steel surface. The method leverages the DenoSeg deep learning network for robust bubble segmentation under challenging conditions (reflected light, optical distortions) and introduces an algorithm for tracking bubbles and calculating time-dependent characteristics.

The system identifies and classifies bubbles into three types (isolated, clustered, and pulsating) to extract the essential boiling parameters, including nucleation site density, surface area fraction, maximum diameter, and nucleation frequency. Validation against manual key frame analysis confirms the system's accuracy. The results not only verify the significant prevalence of clustered and pulsating bubbles but also, thanks to extensive data processing, reveal trends hidden by stochastic noise, such as the growth of the maximum diameter of clusters with increasing surface temperature. The developed tool provides a reliable foundation for building predictive heat transfer models for non-stationary boiling regimes.

**Index Terms** — Nucleate boiling, machine learning, image segmentation, time-averaging, nucleation site density, maximum bubble diameter, nucleation frequency.

## I. INTRODUCTION

Nucleate boiling in a flow of subcooled liquid is one of the most effective heat removal methods, with widespread applications in power engineering, electronics cooling, and other fields used three CNN models to segment overlapping bubbles, followed by a generative adversarial network (GAN) for hidden bubble part reconstruction [1]. However, boiling properties under non-stationary regimes involving rapid heater temperature changes remain insufficiently studied [2–4].

In recent decades, high-speed videography has been increasingly used to investigate nucleate boiling characteristics. It is impossible to extract parameters of individual bubbles and statistical boiling characteristics from the resulting large volumes of video data without modern automated image and video processing tools [5–10].

The objective of this work is to develop an automated system for identifying bubbles on the heater surface in high-speed video frames captured in reflected light under non-stationary heating conditions, and to obtain characteristics of isolated, clustered, and pulsating bubbles.

## II. LITERATURE REVIEW

Numerical modeling of heat and mass transfer during boiling is a powerful tool for understanding underlying mechanisms [4, 11–13]. Boiling heat flux correlations rely

\* Corresponding author.

E-mail: polinakhan@isem.irk.ru

DOI: [10.25729/esr.2025.04.0006](https://doi.org/10.25729/esr.2025.04.0006)

Received November 14, 2025. Revised November 15, 2025.  
Accepted December 9, 2025. Available online December 29, 2025.

This is an open-access article under a Creative Commons Attribution-NonCommercial 4.0 International License.

© 2025 ESI SB RAS and authors. All rights reserved.

on experimentally determined characteristics such as nucleation site density, bubble diameter, and frequency [14, 15]. Generalizing these correlations for non-stationary, high-temperature-rise-rate regimes remains a significant challenge.

When acquiring new experimental data, it is essential to account for the stochastic nature of vapor generation and the extremely wide parameter scatter of individual bubbles coexisting under identical conditions [16–19]. Measuring the lifetime and dimensions of individual bubbles with sufficient accuracy, while simultaneously gathering statistical data on a sufficiently large number of bubbles, requires processing tens of thousands of bubble images across thousands of frames. Consequently, it is not surprising that with the widespread adoption of high-speed videography in nucleate boiling experiments, methods for machine-assisted processing of video frames have been actively developed.

Heuristic algorithms based on threshold binarization, edge detection, or background subtraction have in some cases allowed for the automation of nucleate boiling video processing [5, 20, 21]. Dark bubbles on a light background are typically obtained when filming in transmitted light using a transparent heater [22, 23]. However, it is well-established that the surface roughness and wettability of the heater, as well as its thickness, heat capacity, and thermal conductivity, have a profound influence on boiling characteristics and the removed heat flux. Therefore, it is essential to obtain experimental data with heater properties that closely approximate those of the heat-transferring surfaces in industrial heat exchangers. Bubbles on a steel heater surface in reflected light are visible to the human eye because they create glares and refract light; however, they do not differ from the background in intensity level and often lack distinct boundaries.

In some cases, algorithms based on correlating video frames with pre-selected bubble templates have shown sufficient effectiveness [24, 25]. The method for cross-correlation of successive video frames is used in the PIV (Particle Image Velocimetry) method for studying the motion of bubbles with more or less constant sizes and shapes [26]. However, cross-correlation is computationally expensive. More importantly, it is poorly suited for bubble clusters, which exhibit immense diversity in forms and structures.

More flexible methods for bubble identification are machine learning techniques implemented in various neural network models. Convolutional Neural Networks

(CNNs) have demonstrated strong performance [6, 7, 9, 10]. Compared to a multilayer perceptron, a CNN contains far fewer weights, making it less resource-demanding and less prone to overfitting. There are several recent works on application of models based on You Only Look Once (YOLO) architecture to detection of bubbles in bubbly flows [8, 27]. Hessenkemper et al. [28] used three CNN models to segment overlapping bubbles, followed by a generative adversarial network (GAN) for hidden bubble part reconstruction.

Nevertheless, preparing a sufficient amount of labeled data for training a deep neural network from scratch is a task as labor-intensive as manually processing a series of experiments. One way to overcome this obstacle is to use pre-trained neural networks, which may require only a few dozen images specific to a given experiment for fine-tuning. This approach is proposed by the authors of the VideoSAM model for segmenting the vapor phase in high-speed video frames [29, 30]. Another approach is unsupervised learning. It is used, in particular, in the DenoiSeg (Denoising & Segmentation) model [31], where the same network is trained to produce both a segmented image and an image denoised from random noise at different outputs. The segmentation output is trained in a supervised manner, while the denoising output is trained unsupervised. There are also examples of successful training of a neural network model designed for recognizing individual bubbles in bubbly flow on generated images [7].

Most existing heat transfer models for nucleate boiling assume that bubble interaction is negligible until at least one-third of the heater surface is covered and can therefore be disregarded. However, several studies [32, 33] have demonstrated that bubbles can activate nearby nucleation sites, meaning bubble clusters can form at the very early stages of boiling. The shape of clustered bubbles is far from spherical, and their size may not correspond to the amount of heat withdrawn from the heater for a given bubble, as heat and vapor transfer occurs between bubbles. In addition to isolated and clustered bubbles, the authors of [33] identified pulsating bubbles. Once formed, these bubbles remain on the surface for 10 to 100 times longer than ordinary bubbles, periodically growing and shrinking in size.

This work tests the hypothesis of the suitability of available neural network architectures, particularly DenoiSeg, for automating the processing of non-stationary boiling videos on an opaque heater. The developed

automated system is validated by comparison with manual processing results. In doing so, it verifies previous conclusions based on manual processing results, regarding the significant proportion of clustered and pulsating bubbles at all stages of nucleate boiling.

### III. METHODOLOGY

#### A. Process Outline

During the experiment on non-stationary boiling, high-speed videography of vapor structures on the heater surface was performed. Each experimental run was defined by two key parameters: the flow subcooling ( $\Delta T_{sub}$ ) and the heater temperature rise rate. The temperature rise rate, which reaches up to 16 000 K/s in this study, was determined relying on the average power generated by the electric current passing through the heater.

The entire processing pipeline for the video frame sequence from a single experiment consisted of three stages:

1. Neural network-based segmentation to define two classes (background and vapor phase).
2. Bubble detection and cataloging.
3. Calculation of time-dependent, averaged boiling characteristics.

In this process, bubbles were accounted for separately according to three types: isolated, clustered, and pulsating.

#### B. Experimental Setup

The experimental data were obtained at the “High-Temperature Circuit” Multi-Access Research Center. A description of the facility and the results of processing individual experiments are provided in [33, 34]. The automated high-speed video frame processing system developed in this study was tested using experimental data for water bubble boiling, characterized by a subcooling of 23–103 K at a pressure of 0.29 MPa, on a technically smooth (machined) steel surface with a maximum roughness of 4  $\mu\text{m}$ , and at an average flow velocity of 0.52 m/s.

Videography of the vapor structures on the heater surface was performed through the opposite transparent channel wall and a 3 mm layer of water. One or two high-power LED lamps were used for illumination. The light passed through the same transparent wall from above and below the camera at an angle of approximately 45° to the heater surface. This configuration created one or two glares on each isolated bubble and, due to the scattered light component, made it possible to distinguish the overall

structure of the background and vapor cavities.

A Phantom V2012 high-speed camera was used for filming, with a resolution of 5.5  $\mu\text{m}$  per pixel. This setup allowed for the recording of bubbles with a size of approximately 10  $\mu\text{m}$  and larger. Frame rates of up to 350 000 Hz were available at a resolution of 128×128 pixels. However, preliminary video analysis established that no bubbles with a lifetime of less than 10  $\mu\text{s}$  were observed; it was therefore decided to reduce the frame rate to 180 000 Hz. This allowed for capturing frames with a size of 256×256 pixels, corresponding to a 1.4 mm × 1.4 mm area on the heater surface plane. The size of individual bubbles on the surface did not exceed 0.3 mm.

For subsequent image segmentation and vapor structure identification, frames were extracted from the video of each experiment, covering the period from the appearance of the first bubble,  $\tau_{ONB}$  (Onset of Nucleate Boiling) until the moment when vapor agglomerates detached from the surface, moved out of the depth of field, and began to obscure other bubbles nucleating on the surface.

#### C. Neural Network-Based Segmentation

The identification system was based on the DenoiSeg neural network architecture [31], which exists in two forms: as a plugin for ImageJ and as a Python module. This work utilized the ImageJ plugin, extended with a macro for batch processing of video frames. The DenoiSeg neural network is a U-Net architecture with four outputs, three of which are dedicated to segmentation, and the fourth to denoising. The target output for the denoising branch is generated automatically, and this output is used for training on unlabeled images. This process adjusts the network's weights that constitute the feature maps, ultimately improving the segmentation results as well.

Our analysis, based on training the network on diverse experimental video datasets, indicates that a segmentation accuracy of  $\geq 95\%$  requires a model specialized for a single surface type. For a given surface, the training data can encompass variations in key parameters such as flow subcooling, heater temperature rise rate, and video capture settings (illumination, focus, exposure, framing). The total training dataset comprised 491 images, of which 68 were annotated. Another 35 annotated images were used for validation and to prevent network overfitting.

When tested on boiling frames from a structured surface, the model trained on data from a technically smooth surface detected approximately 70% of bubbles. While the Python implementation of the DenoiSeg model

allows for adaptation or fine-tuning to address this, the ImageJ plugin version lacks this functionality. Training a new model from scratch for the structured surface is therefore a viable alternative, especially since the process required less than 10 hours on a PC equipped with a single NVIDIA GeForce RTX 4060 Ti GPU.

Figure 1 provides an example of the visual validation of the trained model, showing a comparison of the original frames with their corresponding manually labeled frames and the frames obtained via segmentation by the trained neural network. Although noticeable differences exist between the manual labeling and the results of the automatic segmentation, the statistical characteristics of the bubbles do not exhibit significant distortion.

Furthermore, in the frames marked with numbers 1, 2, and 3, the neural network detected even small bubbles. In the left part of the original frame 3, optical distortions are present, caused by the movement of fluid layers at different temperatures, which had developed during the slow heating process. This did not hinder the automatic identification of bubbles in this area. Frame 4 features large bubbles with a pronounced dry spot area, where the heater surface is visible without any distortion. The neural network misidentified these areas as background. Nevertheless, the overall error rate across various conditions ranged from 0.5 to 5%.

#### D. Bubble detection and cataloging

The next step after image segmentation was to compile, for each experiment, a list of all bubbles that existed from the onset of vapor generation until the detachment of large vapor agglomerates. The characteristics determined for each bubble included its type, the coordinates of the center of mass of its two-dimensional image at the moment of nucleation, the initial and final frames, the maximum achieved size, lifetime, and nucleation frequency.

The maximum achieved size (effective diameter)  $D_j$  of an individual bubble was determined based on the maximum area  $A_j$  reached during its lifetime:

$$D_j = \sqrt{\frac{4A_j}{\pi}}. \quad (1)$$

The bubble lifetime, in seconds, was calculated as the lifetime in frames divided by the frame rate. Since bubble interactions made re-nucleation at the same site infrequent, determining the waiting time for each individual bubble was not feasible. Therefore, the nucleation frequency  $f_j$  of an individual bubble was defined as the reciprocal of its lifetime.

These individual characteristics were determined by analyzing the intersections of regions (objects) marked as vapor (white) across consecutive frames, starting from the frame preceding the appearance of the first bubble. Three bubble types were identified: isolated (also referred to as single), clustered, and pulsating.

**An isolated bubble** is the most common type considered in the majority of boiling models. It refers to a bubble that nucleates in an area not occupied by other bubbles due to the accumulation of sufficient surface superheat near an active site, undergoes phases of hydrodynamic and thermal expansion, then shrinks and either condenses on the surface or detaches.

In image processing, an isolated bubble is algorithmically defined as a continuous sequence of segmented objects that do not undergo merging or splitting. The sequence must satisfy two criteria: 1) the intersection between two consecutive objects is non-empty, and 2) the displacement of their centroids does not exceed 5 pixels. This threshold, corresponding to a velocity of approximately 5 m/s, was determined through visual inspection of the video dataset. The first object in such a sequence has no intersection with any object in the preceding frame.

**Clustered bubbles** are defined by their participation in interactions such as merging, splitting, or rapid displacement. These processes enable vapor and heat exchange between bubbles, so a bubble's size may no longer directly reflect the energy received from the heater alone. While touching yet distinct bubbles can be identified during manual frame-by-frame analysis, they appear as a single, irregularly shaped region in a segmented binary image, representing a bubble cluster.

Unlike an isolated bubble, a cluster exhibits three critical features that affect its contribution to heat transfer models: 1) internal vapor and heat transfer, 2) a complex, non-spherical shape with a thickness significantly smaller than its in-plane diameter, and 3) a shortened effective lifetime, typically confined to the interval between interactions.

**A pulsating bubble** is defined by its resumption of growth after beginning to shrink, undergoing multiple such cycles until it is displaced or absorbed by a cluster. It typically attains a smaller maximum size and exhibits a lower growth rate compared to an isolated bubble at the same nucleation site. This is because, lacking a dormant phase for energy accumulation, it cannot initiate the rapid hydrodynamic growth and micro-layer evaporation characteristic of an isolated bubble. Consequently, an

individual pulsating bubble transfers less heat. Despite this, the collective contribution of pulsating bubbles to the total heat flux can be significant, as their small and stable sizes allow for high surface packing density.

In automated processing, a pulsating bubble is identified similarly to an isolated one, with a key distinction: the sequence starts from an object intersecting a single, shrinking bubble from the previous frame. Consequently, each growth-shrinkage cycle was logged as a separate “bubble” entry in the dataset.

### E. Calculation of Time-Dependent, Averaged Boiling Characteristics

Surface cavities contribute to the population of active nucleation sites as the increasing surface temperature expands the range of permissible curvature radii [35]. However, they can be activated earlier upon contact with another bubble. On the other hand, once the required surface temperature is reached, a bubble might be absent from a nucleation site for a stochastic waiting period. Furthermore, on an engineered surface, the spatial distribution of cavities with different curvature radii is random. For these reasons, even the most precise bubble count on a single frame from a small surface area does not provide reliable data on the overall nucleation site density on the heater at a given temperature. Further increasing the camera's field of view is only possible by reducing the frame rate. Therefore, the hypothesis of equivalence between spatial and temporal averaging with a certain time step was adopted; that is, the ergodicity of the bubble system on the heater surface was assumed. The temporal averaging window,  $\Delta t$ , must exceed the average bubble lifetime (approximately 0.03 ms) and be less than the time required for the surface temperature to increase by 10 K (0.5 ms at a surface temperature rise rate of 20 K/ms).

The boiling characteristics in each individual experiment were calculated for time instances  $t \in \left[ \tau_{ONB} + \frac{\Delta t}{2}, \tau_{ONB} + \Delta t_1, \tau_{ONB} + \frac{\Delta t}{2} + 2\Delta t_1, \tau_{ONB} + \frac{\Delta t}{2} + 3\Delta t_1, \dots, \tau_{OSV} - \frac{\Delta t}{2} \right]$ , where  $\Delta t_1 \leq \Delta t$ . This study used values of  $\Delta t = 0.55$  ms and  $\Delta t_1 = 0.16$  ms. Statistical processing was performed for four bubble categories:  $S$  – single (isolated),  $C$  – cluster,  $P$  – pulsating,  $A$  – all. The last category is the union of the first three. The processing yielded the following time-dependent functions: nucleation site density,  $N_{a,l}(t)$ , maximum diameter,  $D_{m,l}(t)$ , nucleation frequency,  $f_{b,l}(t)$  and fraction of surface area occupied by bubbles,  $F_{v,l}(t)$ , where  $l \in \{S, C, P, A\}$ . The

values of these functions for each bubble category  $l$  and time  $t$  were determined based on a sublist  $J_l(t)$ , comprising all bubbles of category  $l$  present in at least one frame from

$i_0(t) = \left( t - \frac{\Delta t}{2} \right) f_c$  to  $i_1(t) = \left( t + \frac{\Delta t}{2} \right) f_c - 1$ , where  $f_c$  is the

frame rate. Henceforth in this subsection, the index  $l$  is omitted for brevity, as the processing was performed identically and independently for each category.

When compiling the sublist of bubbles for the category under consideration, the value  $p_j(t)$  – the fraction of frames within the interval  $[i_0(t), i_1(t)]$ , in which the bubble with index  $j$  was present – was calculated for each  $j$ -th bubble. Note that  $0 < p_j(t) \leq 1$ . The nucleation site density at time  $t$  is simply the sum of  $p_j(t)$ , divided by the frame area  $A_c$ :

$$N_a(t) = \frac{1}{A_c} \sum_{j=1}^{J(t)} p_j(t). \quad (2)$$

In particular, if all  $J(t)$  bubbles existed throughout the entire considered interval, then  $N_a(t) = \frac{J(t)}{A_c}$ . If all  $J(t)$  bubbles appeared strictly sequentially from a single nucleation site, then  $N_a(t) = \frac{1}{A_c}$ .

When calculating the averaged maximum diameter values, the maximum diameter of each bubble was multiplied by a weighting factor equal to  $p_j(t)D_j^3$ , because the amount of heat transferred from the heater surface to the liquid during the formation and subsequent condensation of a given bubble is approximately proportional to its volume. Thus,

$$D_m(t) = \frac{\sum_{j=1}^{J(t)} p_j(t) D_j^4}{\sum_{j=1}^{J(t)} p_j(t) D_j^3}. \quad (3)$$

The nucleation frequency, as a characteristic of an individual bubble, was also averaged using a weight proportional to its volume and presence fraction  $p_j(t)$ :

$$f_b(t) = \frac{\sum_{j=1}^{J(t)} p_j(t) f_j D_j^3}{\sum_{j=1}^{J(t)} p_j(t) D_j^3}. \quad (4)$$

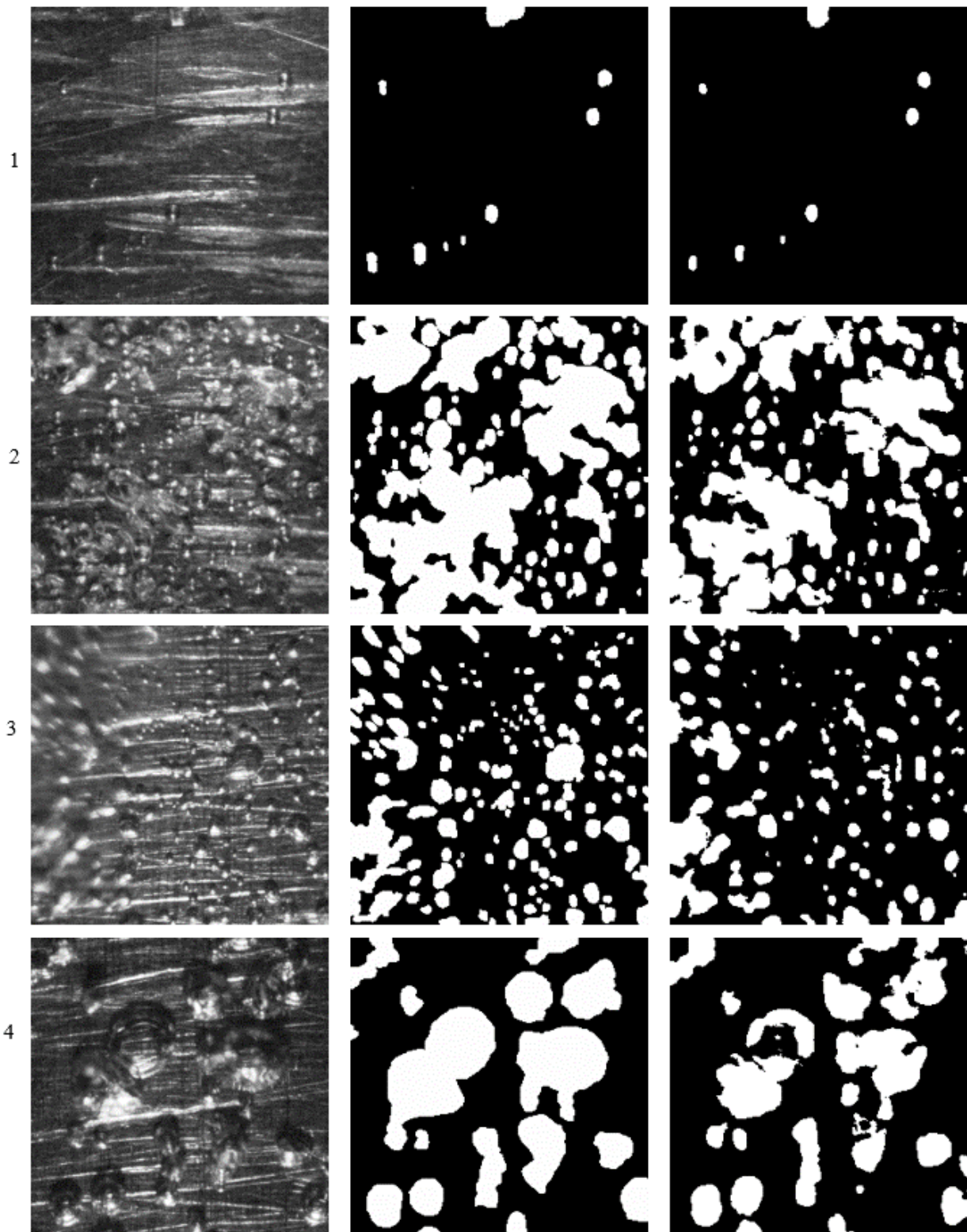


*Fig. 1. Validation of individual video frame segmentation results. Raw: original frames, gt: manually labeled ground truth, NN-result: neural network segmentation result. Experimental conditions: 1, 2 –  $\Delta T_{sub} = 53$  K,  $dT/dt = 3600$  K/s; 3 –  $\Delta T_{sub} = 103$  K,  $dT/dt = 330$  K/s; 4 –  $\Delta T_{sub} = 23$  K,  $dT/dt = 9900$  K/s.*

The areas occupied by individual bubbles in a single frame are non-intersecting segments. However, when determining the surface area involved in the heat transfer process due to boiling, each bubble was considered with the maximum area it achieved during its lifetime. At the stage of statistical processing of the bubble list, information about the shape of the region covered by the bubble at that moment was unavailable, and it was approximated as a circle with a diameter  $D_j$ . Such circles with maximum diameters for different bubbles can overlap, and this must be accounted for.

To estimate the fraction of area occupied by bubbles as accurately as possible, a two-dimensional array corresponding to all pixels in the frame was created. The array was initialized with zeros. Then, for each bubble from  $J(t)$  the value  $p_j(t)$  was added to all array elements corresponding to pixels within the circle of diameter  $D_j$  centered at the bubble's center of mass, with the constraint that no element value could exceed 1. Subsequently,  $F_v(t)$  was calculated as the sum of all elements in this array, divided by the total frame area in pixels.

#### IV. RESULTS

To validate the developed automated video data processing system, its results were compared with those previously obtained through manual processing. For comparison, two experiments with a high surface temperature rise rate (12 000–16 000 K/s) and flow subcooling of  $\Delta T_{sub} = 23$  K and 103 K were selected.

The manual processing was conducted as follows. In each experiment, approximately 10 key frames (KF) were selected during the initial phase of nucleate boiling. For each key frame, a list of bubbles present in it was compiled. For each bubble, its lifetime, maximum diameter, and type (isolated, clustered, or pulsating) were determined by reviewing the video forward and backward from the key frame. The values of nucleation site density, maximum diameter, nucleation frequency, and the fraction of surface area occupied by bubbles of each type and the generalized "All" category were determined using formulas analogous to those in the previous section, with  $p_j(t) = 1$ .

As is seen in Fig. 2(a, b), the total number of bubbles of all types aligns almost exactly between the automated and manual processing methods. An exception is the  $N_a$  values for  $\tau - \tau_{ONB} > 0.8$  ms at  $\Delta T_{sub} = 103$  K, where manual processing yields higher values. This discrepancy is associated with differences in handling clustered bubbles:

during automated processing, an entire cluster of touching bubbles was counted as a single bubble, whereas during manual processing, bubbles distinguishable in the original frame were counted as separate bubbles of the clustered type. The results of the automated processing, covering a longer time period, allow for determining the limiting value of nucleation site density at which saturation occurs. For both experiments considered, this value was approximately  $90 \text{ mm}^{-2}$ .

The fraction of the heater surface area occupied by bubbles of all types (Fig. 2 (c, d)), and particularly by clustered bubbles, is on average higher in the manual processing results compared to the automated results. The total area occupied by a bubble cluster might have been overestimated during manual processing because the area of each bubble within the cluster was calculated as the area of a circle with a diameter equal to the bubble's largest visible dimension. Although the overlap of these circles was accounted for, the actual overlap might have been greater. Furthermore, as seen in Fig. 2 (a, b, c, d), the automated processing attributes a higher relative contribution to pulsating bubbles and a lower one to single bubbles compared to the manual processing. This is because bubbles that did not fully condense but underwent a sharp change in size or structure during the transition from shrinking to growing were classified as single in the manual processing, whereas in the automated processing they were identified as pulsating.

The averaged maximum bubble diameter (Fig. 2 (e, f)) shows close agreement between the manual and automated processing results, especially for the combined category of all bubble types. Clustered bubbles in the automated processing reach larger sizes within the same time interval, which is associated with the distinction between treating an entire cluster as a single entity versus individual bubbles within a cluster. The discrepancy between these two approaches could have been significantly more pronounced if  $D_m$  represented a simple arithmetic mean. The use of a weighting function proportional to the bubble volume during averaging renders small bubbles within a cluster negligible compared to the single bubble that absorbed them upon merging. The differences in  $D_m$  values for isolated and pulsating bubbles obtained manually and via neural networks are not unidirectional, as they are linked to the differences in bubble type classification.

The most significant discrepancies between the manual and automated processing are observed in the nucleation frequency values (Fig. 2 (g, h)). In principle, a close match

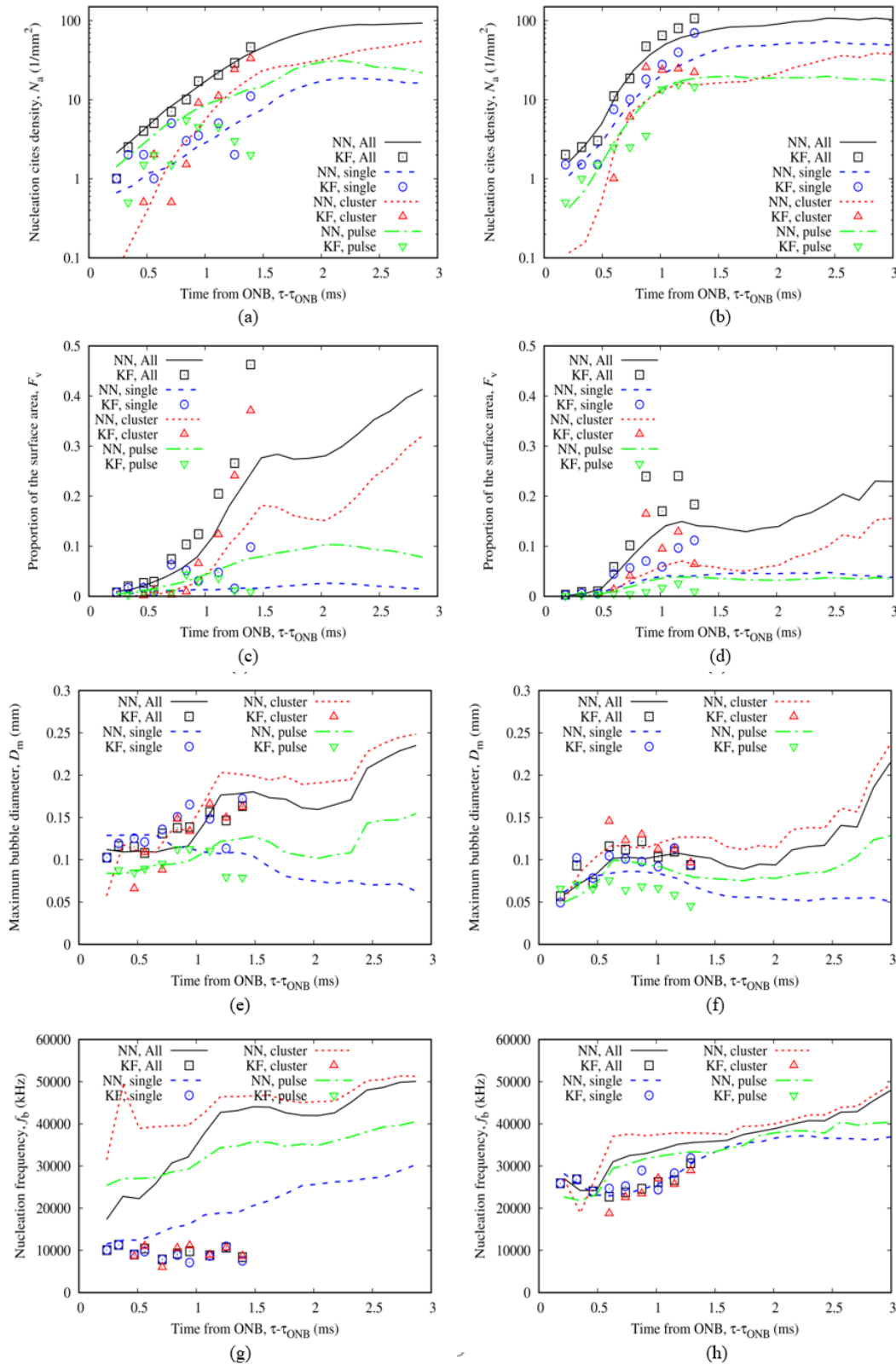


Fig. 2. Verification of neural network (NN) results against manual key frame (KF) analysis for bubble statistics at flow subcoolings of 23 K (a, c, e, g) and 103 K (b, d, f, h). Compared parameters: (a, b) nucleation site density,  $N_a$ ; (c, d) surface area fraction,  $F_v$ ; (e, f) maximum diameter,  $D_m$ ; (g, h) nucleation frequency,  $f_b$ .

for this parameter could only be expected for isolated bubbles. For clustered bubbles, the manual processing yields the lifetime of individual bubbles within a cluster, which characteristically shows little difference from the lifetime of single bubbles. In contrast, the automated processing for clustered bubbles essentially provides not the nucleation frequency, but the frequency of interactions. The lifetime and nucleation frequency of pulsating bubbles were not determined in the manual processing. In the automated processing, this value corresponds to the pulsation frequency.

Thus, the observed discrepancies are minor and largely attributable to differences in the definition of clustered and pulsating bubbles. It should also be noted that, due to the use of temporal averaging over the interval  $\Delta t$  and the presence fraction  $p_j(t)$  for each bubble within this interval in the automated processing, the values of the flow characteristics at the specific time  $t$ , corresponding to a key frame could not exactly match the characteristics derived solely from that key frame, even if the characteristics of individual bubbles had been identified identically. Owing to this temporal averaging, the results of the automated processing provide a more accurate representation of the boiling characteristics averaged over the entire heater surface than the results of the manual processing.

## V. DISCUSSION AND CONCLUSIONS

This study has developed and validated an automated system for quantifying bubble dynamics in non-stationary nucleate boiling on an opaque surface. By integrating the DenoiSeg convolutional neural network for robust segmentation in reflected light with a novel tracking algorithm, the system reliably extracts time-dependent characteristics (nucleation site density, area fraction, maximum diameter, and nucleation frequency), while classifying bubbles into isolated, clustered, and pulsating types.

**Methodological Validation:** Comparison with manual key frame analysis confirmed the system's accuracy. The principal discrepancies are attributed to the more consistent and physically-grounded definitions of bubble interactions within the automated algorithm. Its primary advantage is the ability to process large datasets, yielding statistically robust results and enabling trend analysis that is infeasible manually.

**Physical Insights:** The analysis confirms the significant prevalence of clustered and pulsating bubbles across all tested conditions. Crucially, the automated processing

revealed previously obscured trends, such as the distinct evolution of bubble diameters: while the maximum diameter of clustered and pulsating bubbles increases with surface heating, that of isolated bubbles decreases due to heightened nucleation site density. This underscores the necessity of accounting for bubble type in heat transfer models.

**Method Extendibility:** The developed framework is inherently adaptable. By training the model on new or augmented datasets, it can be applied to segment boiling on structured surfaces or under different system conditions, such as pressure, flow velocity, heater temperature rise rate, and flow subcooling. The subsequent feature extraction would follow the same validated pipeline, ensuring consistency. Applying this methodology to large-scale data collection will enable the systematic identification of key differences in boiling behavior across various surfaces and conditions, distinguishing fundamental trends from stochastic fluctuations.

In conclusion, we have developed and validated an automated tool that enables detailed, physics-based analysis of non-stationary boiling. This methodology paves the way for creating the large, consistent datasets required to refine heat transfer correlations for complex boiling regimes.

## ACKNOWLEDGMENT

The research was funded by the Russian Science Foundation, Grant No. 22-19-00092-II.

## REFERENCES

- [1] C. S. Brooks, T. Hibiki, "Wall nucleation modeling in subcooled boiling flow," *Int. J. Heat Mass Transf.*, vol. 86, pp. 183–196, 2015. DOI: 10.1016/j.ijheatmasstransfer.2015.03.005.
- [2] M. C. Duluc, B. Stutz, M. Lallemand, "Transient nucleate boiling under stepwise heat generation for highly wetting fluids," *Int. J. Heat Mass Transf.*, vol. 47, no. 25, pp. 5541–5553, 2004. DOI: 10.1016/j.ijheatmasstransfer.2004.04.038.
- [3] A. N. Pavlenko, E. A. Tairov, V. E. Zhukov, A. A. Levin, A. N. Tsoi, "Investigation of transient processes at liquid boiling under nonstationary heat generation conditions," *J. Eng. Thermophys.*, vol. 20, no. 4, pp. 380–406, 2011. DOI: 10.1134/S1810232811040060.
- [4] A. Levin, P. Khan, "Intensification of non-stationary nucleate boiling at increasing flow velocity," *Heat Transf. Eng.*, vol. 43, no. 3–5, pp. 388–396, 2022. DOI: 10.1080/01457632.2021.1874682.

- [5] V. Serdyukov, I. Malakhov, A. Surtaev, "High-speed visualization and image processing of sub-atmospheric water boiling on a transparent heater," *J. Vis.*, vol. 23, no. 5, pp. 873–884, 2020. DOI: 10.1007/s12650-020-00660-z.
- [6] T. Haas, C. Schubert, M. Eickhoff, H. Pfeifer, "BubCNN: Bubble detection using Faster RCNN and shape regression network," *Chem. Eng. Sci.*, vol. 216, Art. no. 115467, 2020. DOI: 10.1016/j.ces.2019.115467.
- [7] I. Poletaev, M. P. Tokarev, K. S. Pervunin, "Bubble patterns recognition using neural networks: Application to the analysis of a two-phase bubbly jet," *Int. J. Multiph. Flow*, vol. 126, Art. no. 103194, 2020. DOI: 10.1016/j.ijmultiphaseflow.2019.103194.
- [8] L. Lentz, D. Hüne, S. Handrich, C. Niems, T. Gimpel, "Bubble Evolution Detector B.E.D. – A neural network-based approach to accurately detect, classify, and evaluate gas bubbles captured by a high-speed camera on textured surfaces," *J. Open Res. Softw.*, vol. 13, no. 1, Art.no. 5, 2025. DOI: 10.5334/jors.505.
- [9] A. Seredkin et al., "Pattern recognition for bubbly flows with vapor or gas-liquid interfaces using U-Net architecture," in *Proceedings - 2020 Science and Artificial Intelligence Conference, S.A.I.ence 2020*, Novosibirsk, Russia, 2020, pp. 5–8. DOI: 10.1109/S.A.I.ence50533.2020.9303175.
- [10] J. H. Seong, M. Ravichandran, G. Su, B. Phillips, M. Bucci, "Automated bubble analysis of high-speed subcooled flow boiling images using U-Net transfer learning and global optical flow," *Int. J. Multiph. Flow*, vol. 159, Art. no. 104336, 2023. DOI: 10.1016/j.ijmultiphaseflow.2022.104336.
- [11] S. P. Aktershev, A. A. Levin, I. V. Mesentsev, N. N. Mesentseva, "Self-oscillatory regime of boiling of a highly subcooled liquid in a flow-passage annular duct," *Thermophys. Aeromechanics*, vol. 25, no. 6, pp. 875–887, 2018. DOI: 10.1134/S0869864318060082.
- [12] A. A. Levin, A. S. Safarov, V. M. Chudnovskii, A. A. Chernov, "Modeling of non-stationary temperature field in the neighborhood of the optical fiber end under laser pulse heating," *Interfacial Phenom. Heat Transf.*, vol. 8, no. 1, pp. 25–32, 2020. DOI: 10.1615/InterfacPhenomHeatTransfer.2020032806.
- [13] A. A. Levin, V. F. Chistyakov, E. A. Tairov, "On application of the structure of the nonlinear equations system, describing hydraulic circuits of power plants, in computations," *Bull. South Ural State Univ. Ser. Math. Model. Program. Comput. Softw.*, vol. 9, no. 4, pp. 53–62, 2016. DOI: 10.14529/mmp160405.
- [14] R. L. Mohanty, M. K. Das, "A critical review on bubble dynamics parameters influencing boiling heat transfer," *Renew. Sustain. Energy Rev.*, vol. 78, pp. 466–494, 2017. DOI: 10.1016/j.rser.2017.04.092.
- [15] G. Yang, W. Zhang, M. Binama, Q. Li, W. Cai, "Review on bubble dynamic of subcooled flow boiling-part b: Behavior and models," *Int. J. Therm. Sci.*, vol. 184, Art. no. 108026, 2023. DOI: 10.1016/j.ijthermalsci.2022.108026.
- [16] S. S. Kutateladze, *Fundamentals of heat transfer*. London, UK: Edward Arnold, 1963.
- [17] N. V. Vasiliev, A. Y. Varaksin, Y. A. Zeigarnik, K. A. Khodakov, A. V. Epelfeld, "Characteristics of subcooled water boiling on structured surfaces," *High Temp.*, vol. 55, no. 6, pp. 880–886, 2017. DOI: 10.1134/S0018151X17060189.
- [18] A. A. Levin, P. V. Khan, "Experimental observation of the maximum bubble diameter in non-stationary temperature field of subcooled boiling water flow," *Int. J. Heat Mass Transf.*, vol. 124, pp. 876–883, 2018. DOI: 10.1016/j.ijheatmasstransfer.2018.03.078.
- [19] A. A. Levin, P. V. Khan, "Effect of micro-sized vapor bubbles on heat transfer at different heater temperature rise rate," *Tech. Phys. Lett.*, vol. 50, no. 2, pp. 58–61, 2024. DOI: 10.61011/TPL.2024.02.57987.19762.
- [20] N. Agarwal, M. Lee, H. Kim, "A non-invasive method for measuring bubble column hydrodynamics based on an image analysis technique," *Processes*, vol. 10, no. 8, art. no. 1660, 2022. DOI: 10.3390/pr10081660.
- [21] B. A. Phillips, "Experimental investigation of subcooled flow boiling using synchronized high speed video, infrared thermography, and particle image velocimetry," Ph. D. dissertation, Department of Nuclear Science and Engineering, Massachusetts Institute of Technology, Cambridge, MA, USA, 2014.
- [22] J. Kim, B. Do Oh, M. H. Kim, "Experimental study of pool temperature effects on nucleate pool boiling," *Int. J. Multiph. Flow*, vol. 32, no. 2, pp. 208–231, 2006. DOI: 10.1016/j.ijmultiphaseflow.2005.09.005.
- [23] S. Narayan, A. Srivastava, S. Singh, "Rainbow schlieren-based direct visualization of thermal gradients around single vapor bubble during nucleate boiling phenomena of water," *Int. J. Multiph. Flow*, vol. 110, pp. 82–95, 2019. DOI: 10.1016/j.ijmultiphaseflow.2018.08.012.
- [24] X. Zabulis, M. Papara, A. Chatziargyriou, T. D. Karapantsios, "Detection of densely dispersed spherical bubbles in digital images based on a template matching technique. Application to wet foams," *Colloids Surfaces A: Physicochem. Eng. Asp.*, vol. 309, no. 1–3, pp. 96–106, 2007. DOI: 10.1016/j.colsurfa.2007.01.007.
- [25] P. Zhevnev, P. Khan, A. Mikheev, "Image processing for identification of vapor phase on a heating surface under the nonstationary boiling conditions," *E3S Web of Conferences*, 2019, vol. 114, Art. no. 07006. DOI: 10.1051/e3sconf/201911407006.
- [26] E. Teodori, A. S. Moita, A. L. N. Moreira, "Characterization of pool boiling mechanisms over micro-patterned surfaces using PIV," *Int. J. Heat Mass Transf.*, vol. 66, pp. 261–270, 2013. DOI: 10.1016/j.ijheatmasstransfer.2013.07.033.
- [27] T. Chen, Q. Zeng, "Research on bubble detection based on improved YOLOv8n," *IEEE Access*, vol. 12, pp. 9659–9668, 2024. DOI: 10.1109/ACCESS.2024.3353196.
- [28] H. Hessenkemper, S. Starke, Y. Atassi, T. Ziegenhein, D. Lucas, "Bubble identification from images with machine learning methods," *Int. J. Multiph. Flow*, vol. 155, Art. no. 104169, 2022. DOI: 10.1016/j.ijmultiphaseflow.2022.104169.

- [29] A. Kirillov et al., “Segment Anything,” *arXiv:2304.02643*, 2023. DOI: 10.48550/arXiv.2304.02643.
- [30] C. Maduabuchi, E. Jossou, M. Bucci, “VideoSAM: A large vision foundation model for high-speed video segmentation,” 2024. DOI: 10.48550/arXiv.2410.21304.
- [31] T. O. Buchholz, M. Prakash, D. Schmidt, A. Krull, F. Jug, “DenoSeg: Joint denoising and segmentation,” in *Computer Vision – ECCV 2020 Workshops. Glasgow, UK, August 23–28, 2020, Proceedings, Part I. Lecture Notes in Computer Science Series*, 1st ed., vol. 12535, A. Bartoli, A. Fusiello, Eds. Springer Cham, 2020, pp. 324–337. DOI: 10.1007/978-3-030-66415-2\_21.
- [32] R. L. Judd, A. Chopra, “Interaction of the nucleation processes occurring at adjacent nucleation sites,” *J. Heat Transfer*, vol. 115, no. 4, pp. 955–962, 1993. DOI: 10.1115/1.2911392.
- [33] P. V. Khan, A. A. Levin, “Experimental study of the influence of bubble interaction on their characteristics during transient boiling in a flow of subcooled liquid,” *Thermophys. Aeromechanics*, vol. 31, no. 2, pp. 313–319, 2024. DOI: 10.1134/S0869864324020100.
- [34] A. A. Levin, P. V. Khan, “Characteristics of nucleate boiling under conditions of pulsed heat release at the heater surface,” *Appl. Therm. Eng.*, vol. 149, pp. 1215–1222, 2019. DOI: 10.1016/j.applthermaleng.2018.12.126.
- [35] Y. Y. Hsu, “On the size range of active nucleation cavities on a heating surface,” *J. Heat Transfer*, vol. 84, no. 3, pp. 207–213, 1962. DOI: 10.1115/1.3684339.



**Ilya I. Chupin** is a research assistant at the Laboratory for Dynamic of Steam-generating systems at Melentiev Energy Systems Institute, Russia.



**Alexey S. Safarov** is a junior researcher at the Laboratory for Dynamic of Steam-generating systems at Melentiev Energy Systems Institute, Russia.



**Polina V. Khan** is a senior researcher at the Laboratory for Dynamic of Steam-generating systems at Melentiev Energy Systems Institute, Russia. She received her Ph.D. from Yeungnam University, School of Mechanical Engineering, in 2006. Her research interests include nucleate boiling, unsteady heat transfer, and multiphase flow.



**Anatoliy A. Levin** is a head of the Laboratory for Dynamic of Steam-generating systems at Melentiev Energy Systems Institute, Russia. He received his Ph.D. from Melentiev Energy Systems Institute in 2008 and D.Sc. in Engineering from Melentiev Energy Systems Institute in 2024. His research interests include nucleate boiling, unsteady heat transfer, and mathematical modeling of thermal plants equipment. He is an elected member of the Scientific Council of the International Centre for Heat and Mass Transfer (ICHMT).